Computers and Electronics in Agriculture 200 (2022) 107262

Contents lists available at ScienceDirect

Computers and Electronics in Agriculture

journal homepage: www.elsevier.com/locate/compag

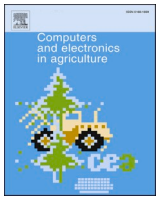

UAV-based multispectral and thermal cameras to predict soil water content – A machine learning approach

László Bertalan [a,*], Imre Holb [b,c], Angelika Pataki [a], Gábor Négyesi [a], Gergely Szabó [a], Annamária Kupásné Szalóki [d], Szilárd Szabó [a]

[a] Department of Physical Geography and Geoinformatics, University of Debrecen, H-4032 Egyetem tér 1. Debrecen, Hungary
[b] Institute of Horticulture, University of Debrecen, Böszörményi út 138, 4032 Debrecen, Hungary
[c] Eötvös Loránd Research Network (ELKH), Centre for Agricultural Research, Plant Protection Institute, Herman Ottó út 15, 1022 Budapest, Hungary
[d] Remote Sensing Centre, University of Debrecen, Böszörményi út 138, 4032 Debrecen, Hungary

ARTICLE INFO

Keywords:
Uncrewed Aerial Vehicles
Pixel value extraction
Model evaluation
Farm size
Regression

ABSTRACT

Soil water content (SWC) estimation is a crucial issue of agricultural production, and its mapping is an important task. We aimed to study the efficacy of UAV-based thermal (TH) and multispectral (MS) cameras in SWC mapping. Soil samples were collected and the SWC content was determined in a laboratory as reference data and four machine learning regression algorithms (Random Forest [RF], Elastic Net [ENR], General Linear Model [GLM], Robust Linear Model [RLM]) were tested for the prediction efficacy, combined with three pixel value extraction methods (single pixel, mean of 20 and 30 cm radius buffer). We found that MS cameras ensured better input data than TH cameras: R^2s were 0.97 vs 0.71, mean-normalized root mean square errors (nRMSE) were 10 vs 25 %, respectively. Best models were obtained by the RF (0.97 R^2) and ENR (0.88 R^2) in case of MS camera. Relationship between SWC and thermal data was exponential, which was incorrectly handled by the GLM (>40 % nRMSE; furthermore, RLM and ENR was not working with only one variable), thus, TH data was acceptable only with the RF (24.4 % nRMSE). Single pixel extraction provided the best input for the estimations, mean of buffered areas did not perform better in the models. Maps provided appropriate SWC estimations according to the nRMSEs, with high spatial resolution. In spite of potential inaccuracies, visualizing the spatial heterogeneities can be a great help to farmers to increase the efficacy of planning irrigation in precision agriculture.

1. Introduction

Success of agricultural production often depends on the availability of water needed for plant growth (D'Odorico et al., 2020). In areas where the amount of precipitation is insufficient, the solution is the irrigation, which can also raise issues (Abdelhaleem et al., 2021; Hao et al., 2022; Négyesi et al., 2021). Irrigation water also can be limited, due to shortage of water in the area, and/or to lack of water with appropriate quality (e.g., high salt content or pollution). In areas where the need for irrigation is high, the evaporation is also high, thus, if the irrigation water has high salt content, it can be desiccated generating unfavorable conditions for plants; or if groundwater has high salt content and its level is raised by the irrigation water also leads to decrease of yields (Abdelhaleem et al., 2021; Bortolini et al., 2018; Hao et al., 2022). Therefore, knowing the required amount of water calculated from the actual water content of soils can help to use the eligible and useful amount of water, leading to a more effective precision farming and water management.

Soil water content (SWC), at farmland level, can be determined by field work in several ways. An accurate method is to collect soil samples from the plots and to use the gravimetric method to determine the water content: the weight of wet soil (collected in the field) and dry soil (dried in a drying chamber at 105 °C) provides possibilities for a gravimetric and as water's density is 1 g/cm^3, it can be converted easily into volumetric water content. Although it is a precise approach, it takes time and requires a laboratory with appropriate equipment and personnel (Little et al., 1998). A faster possibility is provided by using moisture meter devices with probes, e.g., the Time Domain Reflectometry (TDR), but the accuracy is limited by the saturation level of the soils (Romano, 2014). All field-based methods have the problem of the extrapolation of the measured values by inhomogeneities, soil texture, and micro topography (Pye and Tsoar, 2009; Wigmore et al., 2019; Hu et al., 2017;

* Corresponding author.
E-mail address: bertalan@science.unideb.hu (L. Bertalan).

https://doi.org/10.1016/j.compag.2022.107262
Received 24 January 2022; Received in revised form 28 April 2022; Accepted 24 July 2022
Available online 1 August 2022

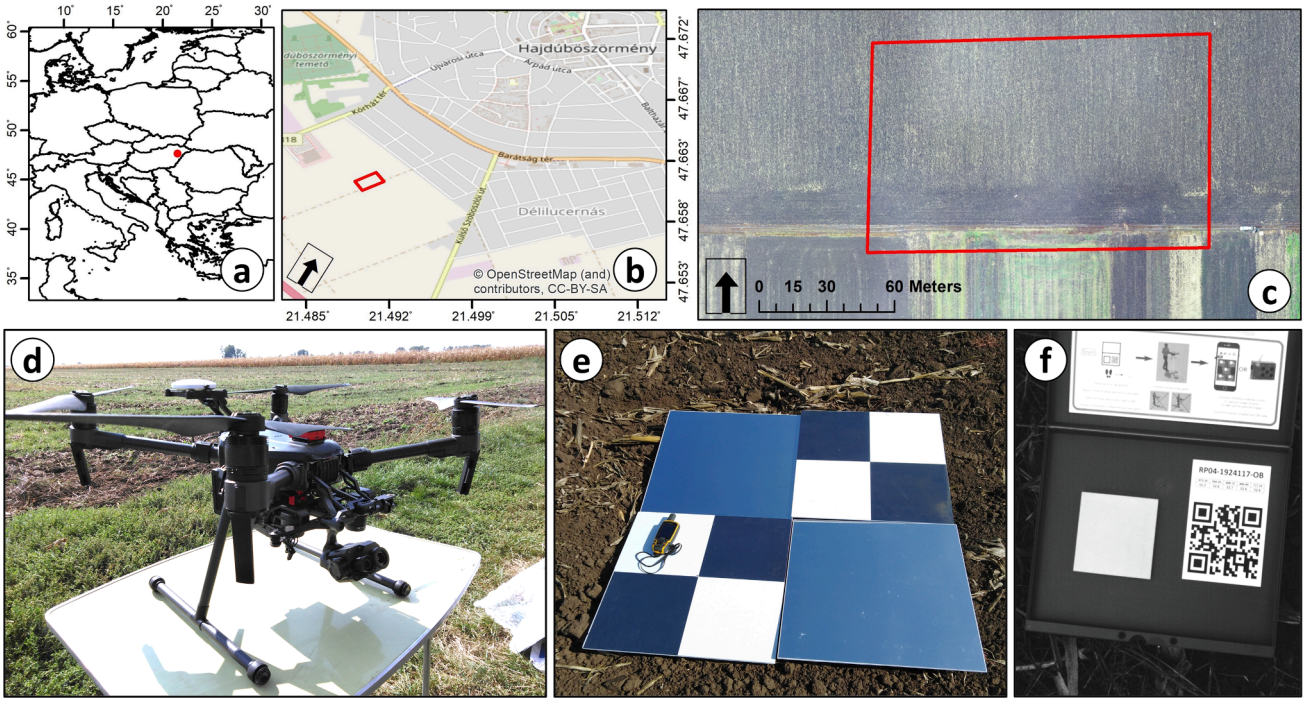

Fig. 1. Location of the study area and parts of the survey equipments: (a) location of Hajdúböszörmény in a European map; (b) location of the sampled agricultural area at Hajdúböszörmény; (c) the red rectangle represents the sampled area; (d) a DJI Matrice M210 UAV + Zenmuse XT2 camera; (e) the specific design of our Ground Control Points (GCP) for mosaicking the thermal imagery; and (f) a MicaSense CRP (Calibrated Reflectance Panel).

Vereecken et al., 2014; Wang et al., 2012). Accordingly, the accuracy of (SWC) maps based on field sampling is a function of the sampling density, and considering that inhomogeneity can be large, real spatial pattern never can be mapped based on a limited number of measurements.

A perspective solution is remote sensing with satellite imagery (Petropoulos et al., 2015; Sabaghy et al., 2018; Tajik et al., 2019; Zhuang et al., 2020) and the cheaper, newly developed devices such as Uncrewed Aerial Vehicles (UAVs) with multispectral and thermal cameras (Wang et al., 2018; Hsu and Chang, 2019; Lu et al., 2020), it also can be a versatile way of SWC mapping. Satellite images had been successfully applied in SWC estimation both using thermal band or optical multispectral bands with the Thermal Optical Trapezoid Model (TOTRAM) (Sadeghi et al., 2017; Yadav et al., 2019) and the Optical Trapezoidal Model (OPTRAM) (Babaeian et al., 2018; Hassanpour et al., 2020), but depending on the required data, the spatial resolutions of these models are 20, 30 and 100 m (Sentinel-2, or Landsat-5 and Landsat-8/9, respectively). If higher spatial resolution is needed, cameras mounted on UAVs are the most effective choices (Tmušić et al., 2020). However, the UAS-based mapping cannot be applied for the same spatial coverage of satellite imagery, but their higher spatial and temporal resolution provide exceptional potentials for soil mapping (Manfreda et al., 2018) especially, when the relative expenses are studied (Matese et al., 2015). The application of fixed-wing UAS models could increase the size of the image acquisition window for extensive mapping purposes too (Mukherjee et al., 2019; Zhang et al., 2021).

Thermal cameras are introduced in previous studies to map SWC using the relationship between the water content and Land Surface Temperature (LST), i.e., specific heat of water is 3–4 times higher than of soil constituents, thus, lower temperature in the soil is an indicator of the presence of water (Petropoulos et al., 2009). Although, this procedure has an increasing literature, and even is used in the practical agricultural SWC mapping, there are limiting factors, too. Thermal cameras have a limited spatial resolution, and this usually cause difficulties at homogenous areas, such as agricultural plots with bare soil (Maes et al., 2017). In these conditions, the traditional Structure-from-Motion (SfM) algorithms may fail through the identification of keypoints for dense image matching, and later, to produce a thermal orthomosaic from the single aerial images (Virtue et al., 2021). Furthermore, the surveyed area is limited by the flight height: too high altitude makes impossible to identify and mark the Ground Control Points (GCPs), which are crucial to georeference the images for aerial triangulation (James et al., 2019). Another issue can be the overheating of the cameras and sensors themselves, and missing images due to possible exposure errors; thus, the final map will not be continuous since even larger image blocks could fail during the alignment (Aragon et al., 2020).

Another possibility is the usage of multispectral cameras. Recent developments on the multispectral sensors led to the application of cameras mounted on UAVs that provide spectral information of the surface from the visible range to near infrared even up to 5–10 bands (Manfreda et al., 2018; Szabó et al., 2018). Synthetic soil image or soil color analysis is a new way of soil property mapping (Al-Naji et al., 2021; Naimi et al., 2021), based on the color of objects and also can be utilized in SWC mapping, too (Lu et al., 2020). UAVs with multispectral cameras ensure the possibility to survey the areas as many times as it is required, and with the calibration of the method, mapping can be possible. Optical imaging can be a new way, based on the fact, that wet soil is associated with darker and dry soil with lighter color, therefore, it may be worth to investigate its efficacy (Al-Naji et al., 2021). Although the OPTRAM also relies on this idea, UAV-based multispectral cameras lack of short-wave infrared (SWIR) bands; thus, the testing is crucial.

Both multispectral and thermal cameras had already been used to explore SWC, but the previous studies partly applied satellite images, and partly spectrometers and cameras under laboratory circumstances (Baumann et al., 2022; Maltese et al., 2010; Minacapilli et al., 2012). Using UAVs combined with both camera types were utilized in this study to extract SWC (Seo et al., 2020), but a comprehensive comparison of efficacy had never been conducted using several machine learning models (MLMs). The application of MLMs on UAV-based SWC data is likely to increase the benefit for precision agriculture in planning soil cultivation or irrigation, however, MLMs options have not been visioned yet in previous studies on SWC data based on UAVs survey in

agricultural practices (Huuskonen and Oksanen, 2018; Bai et al., 2021).

Our aim was to reveal the efficacy of UAV-cameras in SWC mapping on agricultural plot level where the spatial heterogeneity is low. Accordingly, we had the following hypotheses: (i) data of multispectral and thermal cameras can help to predict SWC; (ii) machine learning based regression provide better predictions outperform multivariate linear models, (iii) merging different survey dates increase the variance of the dataset, therefore, the predictions become more accurate, and (iv) buffered areas for spectral sampling provide better reference data than a single pixel, (v) visualization of SWC with optical imaging reveals the spatial heterogeneity in large details.

2. Materials and methods

2.1. Study area

The study area is located at an agricultural plot near to the city of Hajdúböszörmény, Eastern Hungary (Fig. 1/ab). Climate of the region is moderately warm with dry and cold winters (January: −2.1 °C; July: 20.9 °C), the mean annual precipitation is 600 mm (Kovács and Király, 2021). Geological basis of soil formation was the loess according to the aeolian surface formation in the past 2000 years (Lóki, 2020). Soil type was chernozem (udic mollisol group), dominating with a grain size of 0.02–0.05 mm (i.e., loess) fractions, and a high (2–3 %) organic matter content (Soil Survey Staf, 2014). According to the preliminary sampling, the soil conditions were homogenous in the whole sampled area. However, the plot is a part of a larger area of intensive agriculture, where the arable crop at the year of surveys was maize (*Zea mays* L.) managed by the integrated maize production system, but in the year of 2020, it was under ley farming, and all surveys were conducted in stages without vegetation. The local topography of the plot is characterized by a negligible slope.

2.2. Soil sampling and laboratory analysis

We conducted two sampling campaigns parallel with the UAV multispectral cameras (04.06.2019; 14.09.2020) and four samplings with the UAV thermal camera surveys (27.05.2019; 04.06.2019; 10.09.2020; 14.09.2020). We performed only two multispectral surveys because of technical issues of the equipment.

Sampling density was determined by the surveyed area (2.2 ha) (Fig. 1/c) and two sampling teams should have finished the sampling in 1 h (within the timeframe of ± 30 min before and after the survey to minimize SWC difference of potential change in time due to evaporation) with all required steps (sampling, RTK-GPS measurement, temperature measurement). Average distance among the samples was ~ 30 m.

In total, 72 (29 + 11 + 17 + 15 respectively) samples were collected through random distribution from the upper 5 cm of the topsoil and transported into the Complex Environmental Laboratory of Institute of Geosciences (University of Debrecen, Hungary). We determined the gravimetric SWC using a high precision scale as a normalized difference of wet and dry soil.

2.3. UAV surveys and image preprocessing

2.3.1. UAV surveys

The aerial surveys were conducted by a DJI Matrice M210 quadcopter UAV (Fig. 1/d). This flying platform allowed us to combine two different payloads. The thermal infrared (TIR) imagery was captured by a radiometric Zenmuse XT2 dual camera. The TIR sensor of the camera is an Uncooled Vox Microbolometer, having 19 mm focal length that measures the thermal emissions between the 7.5 and 13.5 μm spectra in 9 Hz frame rate. The spatial resolution of the radiometric R-JPEG images was 336 × 256 pixels. The secondary lens provided RGB imagery through a 1/1.7″ CMOS lens with sizes of 12 MP. More detailed information can be found on the manufacturer's website (https://www.dji.com/hu/zenmuse-xt2/specs, 6 December 2021). The multispectral survey was performed by a MicaSense RedEdge-MX sensor that captures data in five different spectral bands (blue, green, red, red edge, near-infrared). More detailed information can be found on the manufacturer's website (https://micasense.com/rededge-mx/, 6 December 2021). The sensor is accompanied by an additional DLS 2 Downwelling Light Sensor that determines the ambient light and sun angle for each band, with the purpose of correcting lighting changes over the study area.

Each aerial mapping flight were operated by the DJI Pilot application. The TIR sensor has relatively low resolution, therefore, significantly higher overlaps were necessary to set up for the flights. We applied both 90 % overlaps for frontlap and sidelap. Both TIR/RGB and multispectral data collection flights had been performed at the altitude of 70 m a.g.l.

The accurate exterior orientation of the SfM processing were ensured by placing 9 GCPs evenly distributed along the study area. The GCP and soil sample coordinates were then surveyed by a Stonex S9i RTK GNSS system having the accuracy of ± 3 cm. With respect to the clear identification of GCPs on the raw TIR imagery, we applied 50 × 50 cm large markers covered by heat mirror foils to shape a standard pattern of GCPs composed by 4 of them (Fig. 1/e).

Each thermal surveys consisted of 380 images, while the multispectrals 1,625 (325 for each band). Both image collections had been processed in Pix4D Mapper v4.5.6. The mean RMSE of the photogrammetric reconstruction were found to be between 0.12 and 0.17 m. The final thermal and multispectral orthomosaics were produced having a Ground Sampling Distance (GSD) of 12.4 and 5.1 cm respectively. The absolute reflectance values had been derived from the raw multispectral bands during the radiometric calibration in Pix4D Mapper using the Calibrated Reflectance Panel (CRP) by MicaSense (Fig. 1/f). A single set of images were captured showing the CRP at the beginning of each multispectral flights.

2.3.2. Spectral value extraction

Spectral values had been extracted in three ways: (i) as single pixel values at sampling points, (ii) as a mean of a 20 cm buffer around the sampling points, and (iii) as a mean of a 30 cm buffer around the sampling points. Buffer distances were chosen according to the rounded GSD of the thermal camera.

2.4. Model building

We applied four machine learning algorithms to predict the SWC using the spectral and thermal data of the cameras. The dependent variable was the gravimetric SWC, the independent variables had been the blue, green, red, red-edge, nir spectral values in case of multispectral camera, and the surface temperature in case of thermal camera.

2.4.1. General Linear model

The applied General Linear Model (GLM) was the multiple regression (MR) in this analysis, which is a common and popular way to reveal the relationship between the dependent and independent variables measured in scale level, and to assess the ability of the independent variables in predicting the dependent variable (Field et al., 2012; Tajik et al., 2012; Ayoubi et al., 2018). The method is based on the ordinary least squares (OLS) to minimize the residual errors. However, MR is regarded sensitive to non-linearity and has assumptions on the normal distribution of the residuals and homoscedasticity. Although most of the cases assumptions are violated, and the results still can be acceptable, these violations are of concerns and should be interpreted. MR was calculated with the caret package in R 4.1.1 (Kuhn et al., 2021.).

2.4.1.1. Robust Linear model. Robust Linear Model (RLM) is an

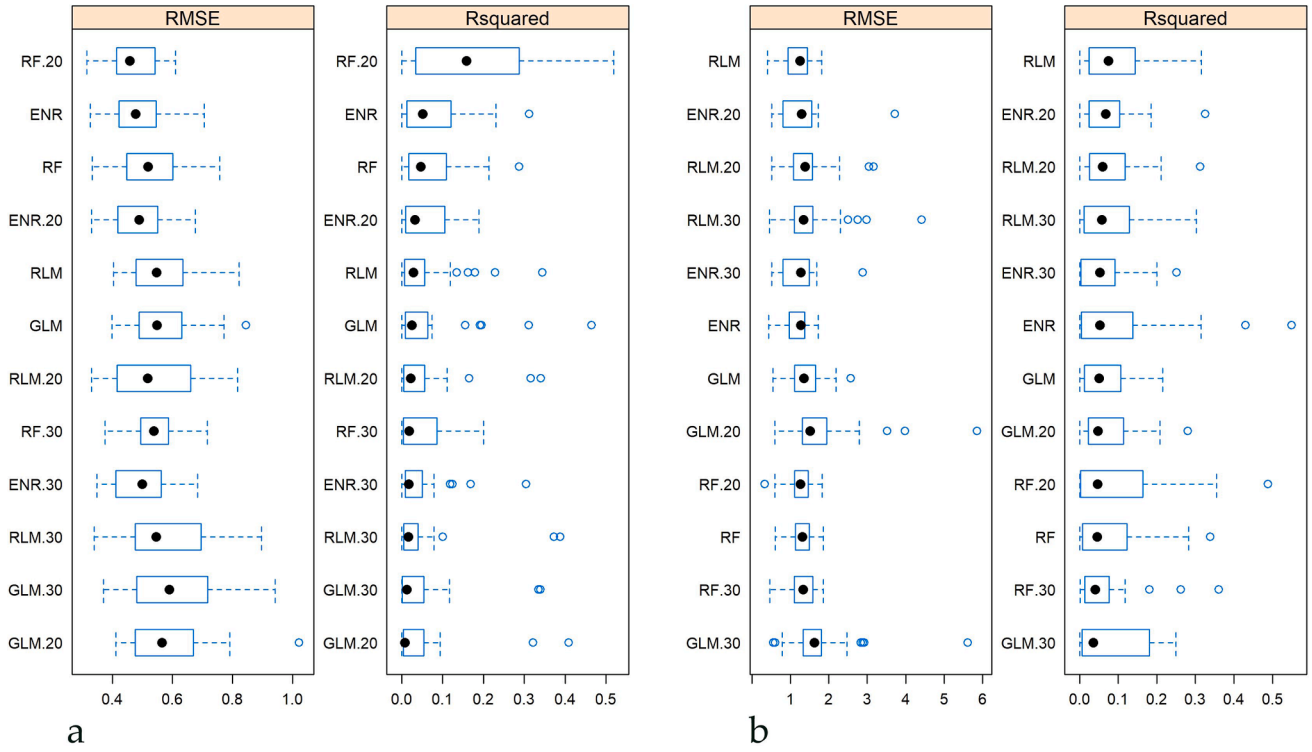

Fig. 2. Root Mean Square Errors (RMSE) and R^2-values (Rsquared) of prediction models based on the spectral data of surveys conducted at 04.06.2019 (a) and at 14.09.2020 (b) based on 30 cross-validated models (GLM: General Linear Model, RLM: Robust Linear Model, RF: Random Forest Regression, ENR: Elastic Net Regression; simple abbreviations: pixel-based data; 0.20: mean of pixels of 20 cm buffer, 0.30: mean of pixels of 30 cm buffer; left and right end of boxes: lower and upper quartiles, •: medians, dashed lines: 1.5-time interquartile ranges).

alternative of MR and is efficient when datasets contain outliers. We applied the RLM version of the M−estimation with the Huber, Hampel and the bisquare weighting. Solution of the equation exploits the iteratively reweighted least squares (Fox, 1997; Robust Regression, 2021). Although this approach is robust, usually efficient only when outliers are present in the data, otherwise MR still performs better (RPubs by RStudio). RLM was calculated and optimized (i.e., selecting the best weighting method with the highest R^2 and lowest residual error) with the MASS (Venables et al., 2002) and caret packages in R 4.1.1.

2.4.1.2. Elastic Net Regression. Elastic Net Regression (ENR) is another way of predictions based on OLS, but the approach uses the augmentation of the OLS loss function with penalizing the parameter estimates. It means that instead of removing any of the independent variables, the algorithm decreases the coefficients. Model complexity decreases and we still can see the contribution of the predictors. ENR is a combination of ridge regression (penalizes the sum of squared coefficients) and lasso regression (penalizes the sum of coefficients' absolute values). ENR is a multivariate model; thus, it was used only with the multispectral data. ENR was calculated with the glmnet (Friedman et al., 2010) and caret packages in R 4.1.1.

2.4.1.3. Random Forest Regression. Random Forest Regression (RF) is a robust algorithm based on large number of decision trees (DTs). Instead of using a single regression tree, RF applies bootstrapping (random sampling from the training dataset with replacement) and runs a new DT on each sample, and finally averages the results (Tajik et al., 2019; Zeraatpisheh et al., 2022; Zeraatpisheh et al., 2021). We applied 500 trees, and maximum number of features at each split had been determined through grid search optimized to find the best performance. RF was calculated with the rpart (Therneau et al., 2019) and caret packages in R 4.1.1.

2.5. Accuracy assessment

The dataset had been split into a training and a testing part in 70–30 %. Training dataset (70 %) was used for model building, and k-fold cross-validation was used as accuracy control, the remaining testing dataset (30 %) was used for predictions on an independent fraction of the reference data, and residual analysis was performed.

2.5.1. K-fold Cross validation

We applied a 3-fold cross-validation with 10 repetitions (RKCV). This procedure works with randomly splitting the training data into k folds (in this case 3), and uses 2 to train a model, and remaining one for testing. Next, another 2-folds are used for training a new model, and another for testing. The sequence ends when all folds were used as testing (Brownlee, 2016). During repetitions the same steps are taken with new randomly split folds. Finally, we had 30 models for each run, and we were able to evaluate the medians and quartiles (LQ: lower quartile, IQR: interquartile range) of the R^2-values and the Root Mean Square Errors (RMSE). We also determined the normalized RMSE (nRMSE; the ratio of the RMSEs and the mean SWCs expressed as percent). RKCV was conducted with the caret package in R 4.1.1.

2.5.1.1. Residual analysis. We determined the predicted SWC using the testing dataset and the models. Residuals (difference of observed and modelled values) were evaluated with the Taylor diagrams and Nash-Sutcliffe model efficiency coefficients (NSE) (Taylor, 2001; McCuen et al., 2006; Gupta and Kling, 2011). Models having NSE < 0.5 are insufficient, between 0.5 and 0.7 are satisfactory, 0.7 and 0.8 are good, and > 0.8 are very good (Moriasi et al., 2015). NSE as a standardized index, which is also independent of input data, was an appropriate tool to compare the model performances, thus, we used it to compare all models having the best model fit (R^2) of both multispectral and thermal data. NSE was calculated in R 4.1.1. with the hydroGOF (Zambrano-

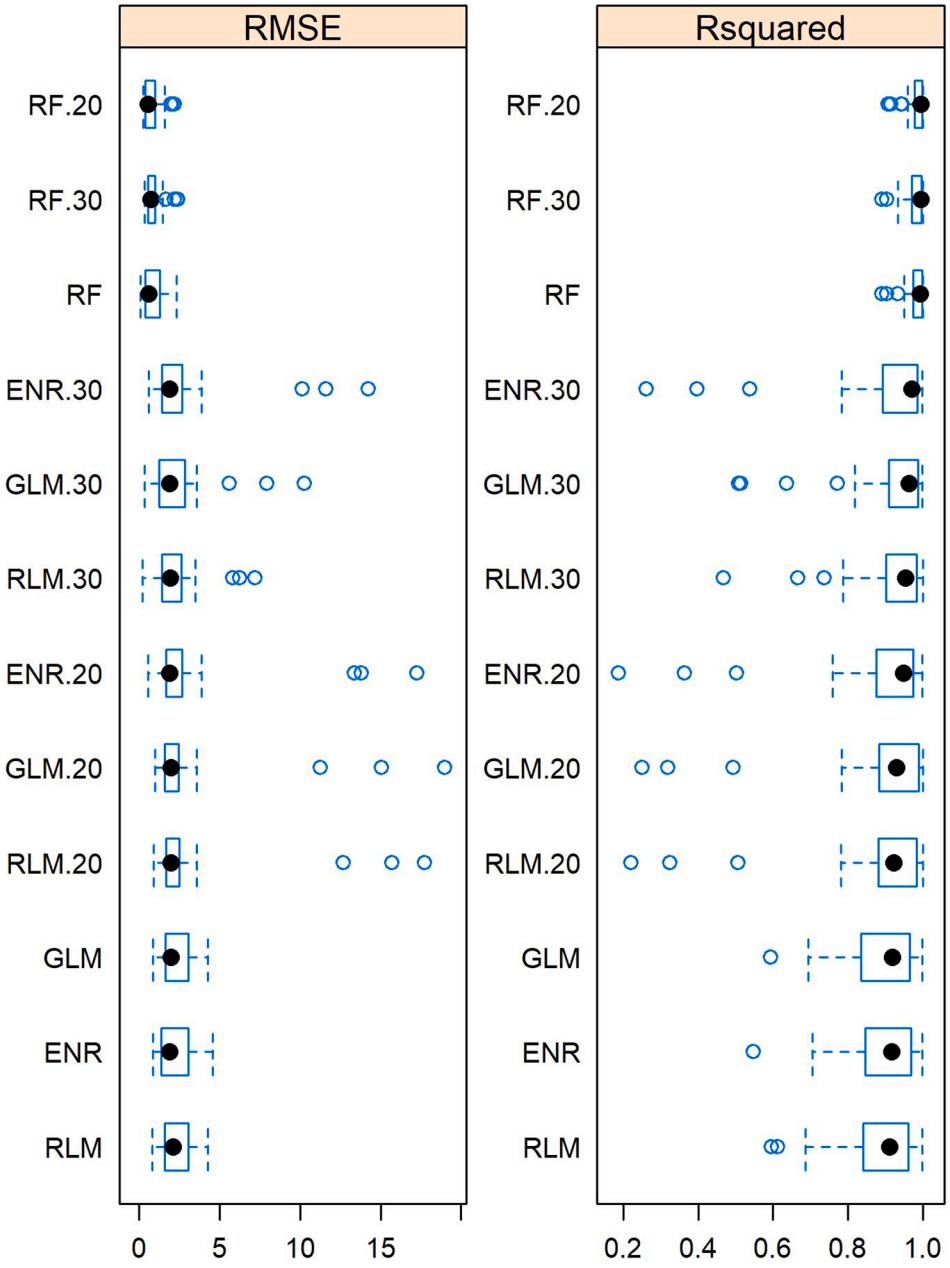

Fig. 3. Root Mean Square Errors (RMSE) and R^2-values (Rsquared) of prediction models using the merged datasets of surveys conducted in the morning and at noon, based on 30 cross-validated models (GLM: General Linear Model, RLM: Robust Linear Model, RF: Random Forest Regression, ENR: Elastic Net Regression; simple abbreviations: pixel based data; 0.20: mean of pixels of 20 cm buffer, 0.30: mean of pixels of 30 cm buffer; left and right end of boxes: lower and upper quartiles, •: medians, dashed lines: 1.5 time interquartile ranges).

Bigiarini, 2020), and the Taylor diagram was generated with the openair (Carslaw and Ropkins, 2012) package in R 4.1.1.

3. Results

3.1. SWC estimation with multispectral data

3.1.1. Evaluation of single surveys with multispectral cameras

Model fits considering the R^2-values were low, usually between 0.001 and 0.02 in case of 04.06.2019, and 0.04–0.05 in case of 14.09.2020 (Fig. 2). Despite that for n the R^2s were lower, the highest value was 0.158 with the RF regression, whilst the best performance for 04.06.2019 it was only 0.074 (RLM). RMSEs were also high, the nRMSEs were between 15.3 % (RF20)-20.1 % (GLM30) in case of 14.09.2020 and between 8.5 % (RF20)-10.9 % (GLM30) with the data captured at 04.06.2019. The maximum nRMSE for the best RF20 model was 20.8 %.

3.1.2. Performance of merged spectral data

Next, we merged the data of the two surveys and found that model fits improved relevantly. Median R^2-values of the 30 models ranged between 0.84 (RLM) and 0.97 (RF20) (Fig. 3). However, regarding the IQRs, only the RF regressions had ensured high performance, even the LQ was at least 0.95 regardless of the buffers (i.e., single pixel, 20 or 30 cm buffer zone). All other models resulted in 0.24–0.64 R^2-values. Regarding the error terms, the median RMSEs were between 10.6 % (RF20) – 93.1 % (GLM20), and for RF models the maximum errors were also lower than 15.6 %.

Using the models based on the combined dataset of the separate surveys, the testing was also performed on the independent testing dataset to compare the modelled and observed values. Although the performance of all models was good. RF also outperformed the other models with the lowest RMSE, highest correlation and almost identical standard deviation with the observed data (Fig. 4). ENR was also efficient, but the GLM's and RLM's modelled values were just slightly weaker than the other models.

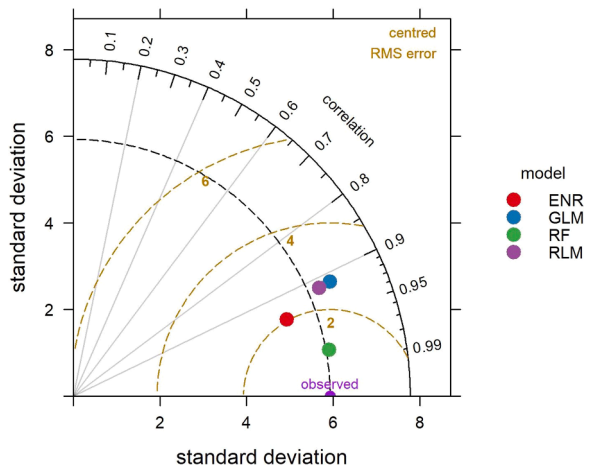

Fig. 4. Taylor diagram of soil water content (%) predicted by Elastic Net Regression (ENR), General Linear Model (GLM), Random Forest Regression (RF) and Robust Linear Regression (RLM) (merged datasets of surveys at 04.06.2019 and 14.09.2020).

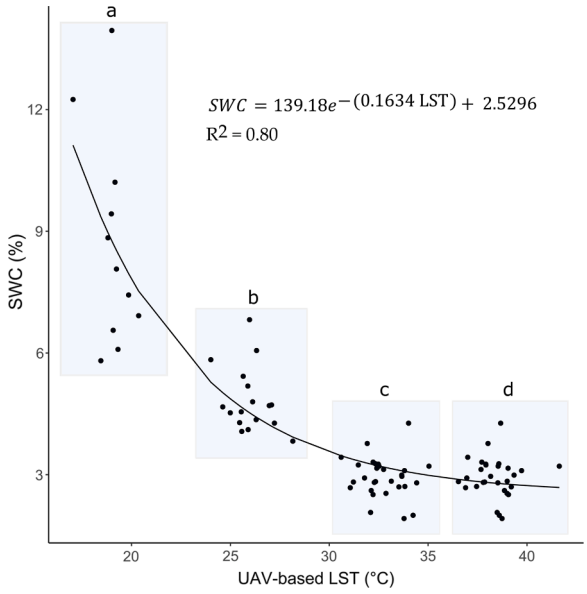

Fig. 5. Relationship between the soil water content (SWC, %) and the land surface temperature (LST, °C) measured by the UAV thermal camera (at the surveys of a: 27.05.2019; b: 04.06.2019; c: 10.09.2020; d: 14.09.2020).

3.2. SWC estimation with thermal camera

3.2.1. Relationship between SWC and land surface temperature

First, we justified the relationship between the temperature measured by the thermal camera and the SWC. We found that the exponential decay function was the most successful approach in this study ($R^2 = 0.80$, while for the linear fit it was only 0.64; Fig. 5). These results showed that it was worth to continue the analysis, but also indicated the possible issues with the classifiers based on linearity (i.e., GLM, RLM).

3.2.2. Single dates

First, we analyzed the surveys by dates and found that the model performance was fluctuating, while medians of the applied models were high R^2 (0.41–0.62) at *date b*, but the simple RMSE can be misleading in Fig. 6 as the corresponding mean SWCs were different. Although the RMSEs were the highest at *date b* and the mean SWC was also the highest, nRMSE was not a favorable one, 34 %. We experienced similarly high nRMSE (30 %) at *date d* with a median R^2 of ~ 0.1. Furthermore, nRMSEs were lower for *date a* and *date c* (19 % and 16 %, respectively), but due to very low R^2-values, we cannot trust in these relationships and use these models as predictors on independent datasets.

3.2.3. Merging data of single surveys

Merging the data of the four surveys provided better models using the RF regression, but the performance of GLM did not improve (RLM and ENR needed at least two independent variables; thus, these models were not applied in this experiment) (Fig. 7). RF provided the highest R^2 (70.9 %), the difference among the pixel-based sampling and the buffer-based means were minimal, but the model fit was slightly better (~2%) for the simple pixel-based solution. However, nRMSE was 24.4 %, but all other metrics showed good model fit and performance. According to the model performance with the testing dataset, modelled and observed values were in good correspondence (Fig. 8). According to the Taylor diagram (Fig. 8), RF was the best classifier, too, with almost 0.9 correlation; the diagram also pointed on the issues of buffer-based means, the RMSEs were 0.3 % higher, closer to 2 %, related to the pixel-based sampling.

3.3. Comparative evaluation of model accuracies

NSEs showed that multispectral surveys provided better results than thermal cameras: only multispectral data ensured models above the benchmark of very good fit (Fig. 9). However, buffering (neither the 20 nor 30 cm radius) around the sampling point did not ensure better predictions than the simple pixel-based data sampling. RF was the best predictor (NSE = 0.97), and the ENR was only slightly weaker (NSE = 0.891). All models using thermal data as independent variable had lower NSEs, even the best model (t.RF) was only 0.67. GLM's efficiency with the thermal data was very low, NSEs were 0.10–0.11.

3.4. Comparison of SWC maps derived from multispectral and thermal cameras

We had run the RF (i.e., best) models on data captured by both camera types and got similar outcomes (Fig. 10). Largest difference was found at the SW part of the area, and in the 20 m range beside the road where the model of multispectral camera data over- and underestimated the SWC related to the model of thermal camera. However, these differences were below 0.5 %, i.e., <15 % relative difference in general.

4. Discussion

SWC is an important information for agricultural production to find the necessity of irrigation or to determine the missing amount of water. Keeping the soils under optimal moisture condition improves the cultivars' yield and decrease the effects of wind erosion on soils (Négyesi et al., 2021). The presence of increasing soil moisture in the first 5 cm of the topsoil indicates a good probability of SWC in the critical root zone i.e., soil layer deeper than 5 cm. On the other hand, the lack of soil moisture in the 5 cm soil layer may indicate a critical decrease of SWC in the root zone deeper than 5 cm soil layer. Root Zone Soil Moisture (RZSM) estimation requires a complex soil mapping methodology. Recent advancements in soil moisture analytical relationship (SMAR) models are continuously developed for revealing the RZSM in a better spatial and temporal scale (Manfreda et al., 2014). However, most of their applications are designed for satellite-based input datasets having more coarse spatial resolution (Baldwin et al., 2017; Baldwin et al., 2019). UAS-based estimation of SWC would lead to the improvement of the RZSM models designed for studies at the plot scale. Remote sensing techniques also help to reveal the spatial heterogeneity of the SWC distribution in a quick and efficient way (Lei et al., 2018). We have had four hypotheses in this research, which were partly justified or

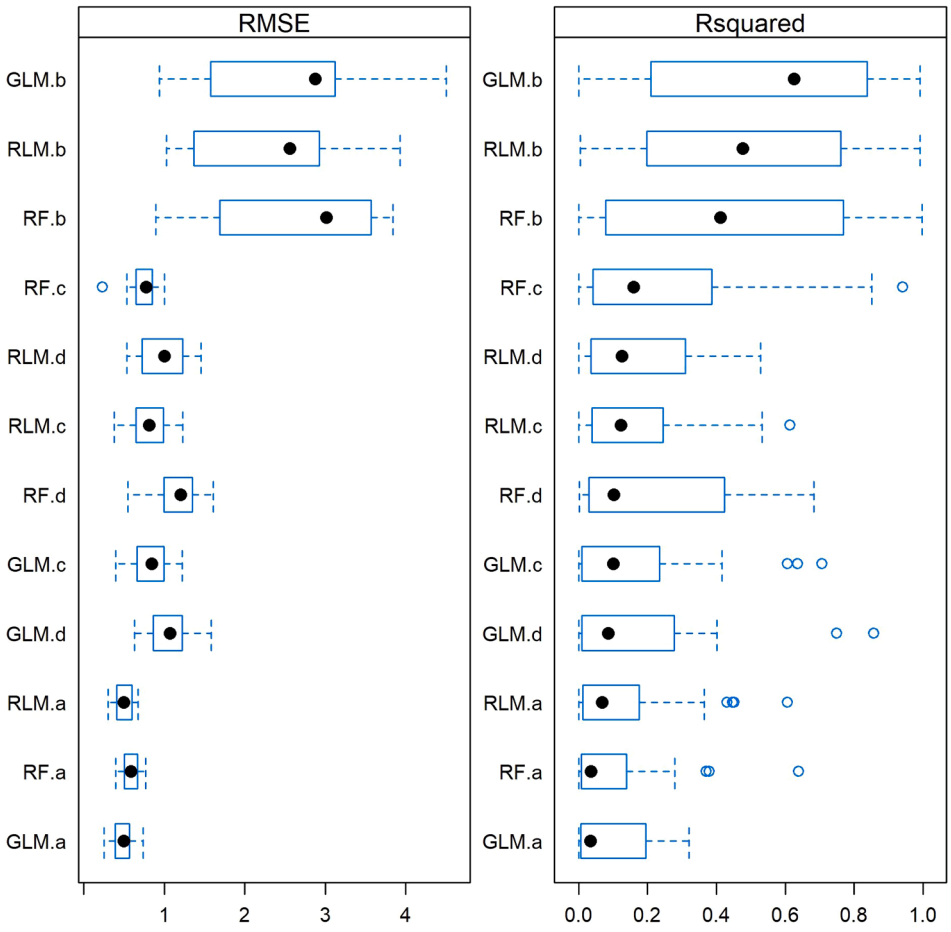

Fig. 6. Root Mean Square Errors (RMSE) and R^2-values (Rsquared) of prediction models using single datasets of surveys conducted at (a: 27.05.2019; b: 04.06.2019; c: 10.09.2020; d: 14.09.2020), based on 30 cross-validated models (GLM: General Linear Model, RLM: Robust Linear Model, RF: Random Forest Regression, ENR: Elastic Net Regression; simple abbreviations: pixel based data; 0.20: mean of pixels of 20 cm buffer, 0.30: mean of pixels of 30 cm buffer; left and right end of boxes: lower and upper quartiles, •: medians, dashed lines: 1.5 time interquartile ranges).

disproved.

We supposed that multispectral imagery can effectively support mapping SWC, and the results justified this theory. Although Bai et al. (2021) found that the maximum R^2 was 0.261 in their research, our results showed a better model performance, having up to 0.9 of R^2. Nevertheless, the methodology of sampling, data capturing, camera and data processing were different, and the difference in model fit calls the attention of the relevance of the topic. The main difference was that we applied the merging of the separate datasets of the single surveys, thus, we increased the variance of both the SWC (different states of soil water content) and the involved spectral data. Ge et al. (2021) applied UAV-based hyperspectral imagery in farmland level (with almost identical size than ours) and found that extreme gradient boost algorithm provided a model fit of $R^2 = 0.921$. Our multispectral data collection contained only 5 bands, but the spectral range was similar (400–1000 nm and 475–842 nm at five narrow bands of 14–57 nm), the hyperspectral did not contain SWIR or thermal bands, and the gained results were also similar with the RF regression.

Considering the RSD (relative standard deviation) values of the predictors (i.e., RGB + red edge + near infrared bands) and the SWC, we found that at the first survey (04.06.2019) the SWC's RSD was 8.2 %, while the spectral bands RSDs were between 18 and 22 %, and the models' OA were 0.1–0.2. At 14.09.2020 the SWC's RSD was 16.8 %, the bands' RSD were between 14 and 17 %, the models' OAs were below 0.1. The merging of the surveys resulted in the SWC's RSD of 61.9 %, and the bands' RSD of 67–74 %, and the models' OAs were above 0.8 or even 0.9. It means that a single survey in a small area cannot ensure enough variability in the data to find the relationship, moreover, indicated very low connection. Accordingly, our suggestion is to perform several surveys on the same area to cover the more possible states of wetness. Color in the same (or neighboring) area can be a good predictor using the visible and near infrared range. This hypothesis was also justified by the residual analysis performed on the independent test data, both the Taylor diagram and the NSE showed that model performance was good.

Regarding the predictors, we found that the RF regression was the most efficient in this study, but ENR was also good in the predictions. GLM and RLM usually had lower performance due to non-linear relationships. Here, the robust characteristic of the RF was the main reason of the best performance, which was not handled appropriately even with the RLM. The relationship was not linear, because the merging itself, both the SWC and the spectral bands had a bimodal distribution, which was not appropriate either for the GLM or the RLM; however, it was not an issue for the RF. The agronomical application of the RF model for estimating SWC may provide a more efficient tool to plan the optimal irrigation water requirement in precision agriculture, as here, one of the key points of irrigation is to determine an optimal water requirement for arable crops (Messina and Modica, 2020).

Data of thermal camera did not provide better predictor than of multispectral camera. Results may be explained by that SWC is dependent upon soil surface temperature including soil thermal characteristics such as thermal diffusivity, heat capacity, emissivity, and thermal conductivity. In addition, all these factors are influenced by soil texture or soil type (Van De Griend et al., 1985; Abu-Hamdeh and Reeder, 2000; Barry-Macaulay et al., 2015; Nikoosokhan et al., 2016; Gu et al., 2021). Previous studies showed that due to soil thermal characteristics, SWC values could be overestimated for clayey soils (Gu et al., 2021). As we did measure on a high clay content, it may influence the overall efficacy of SWC predictions. In this study, median R^2 of the best model for the data of thermal camera was only 70.9 %, and the relating nRMSE was high (almost 25 %). In this case, the merging of the single surveys was

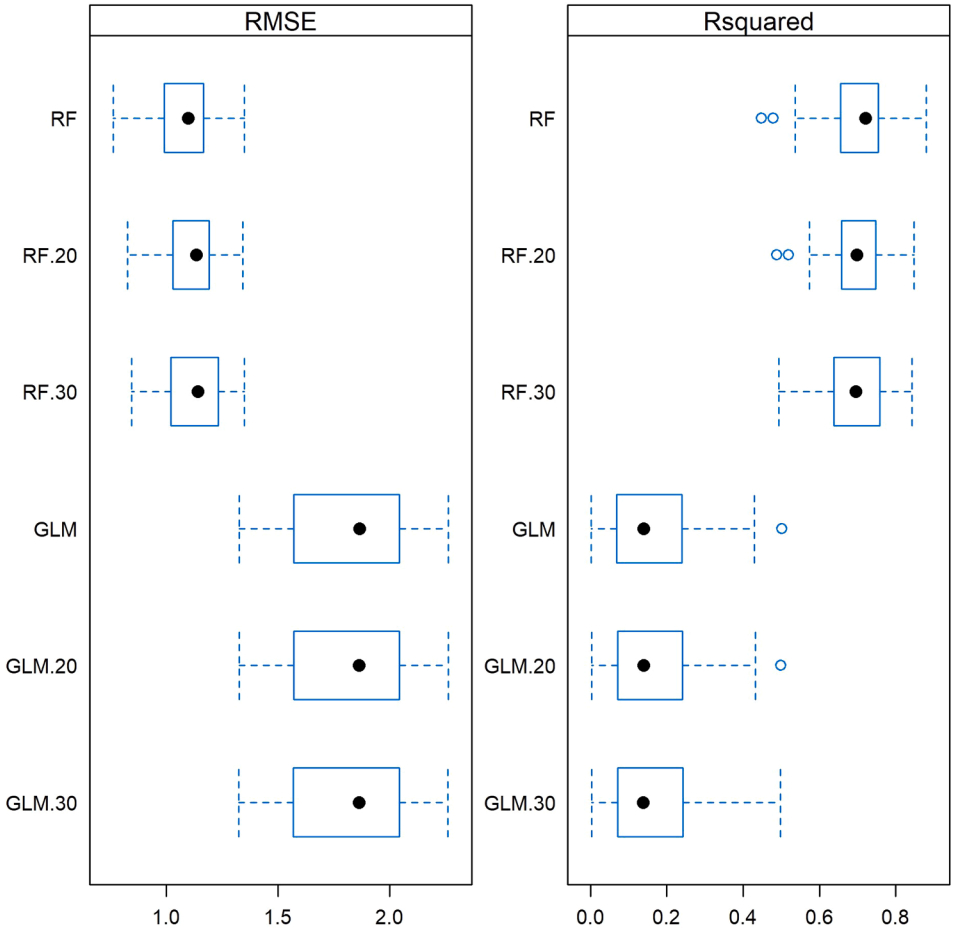

Fig. 7. Root Mean Square Errors (RMSE) and R^2-values (Rsquared) of prediction models using the merged datasets (surveys of 27.05.2019; 04.06.2019; 10.09.2020; 14.09.2020) of single thermal camera surveys, based on 30 cross-validated models (GLM: General Linear Model, RLM: Robust Linear Model, RF: Random Forest regression, ENR: Elastic Net Regression; simple abbreviations: pixel based data; 0.20: mean of pixels of 20 cm buffer, 0.30: mean of pixels of 30 cm buffer; left and right end of boxes: lower and upper quartiles, •: medians, dashed lines: 1.5 time interquartile ranges).

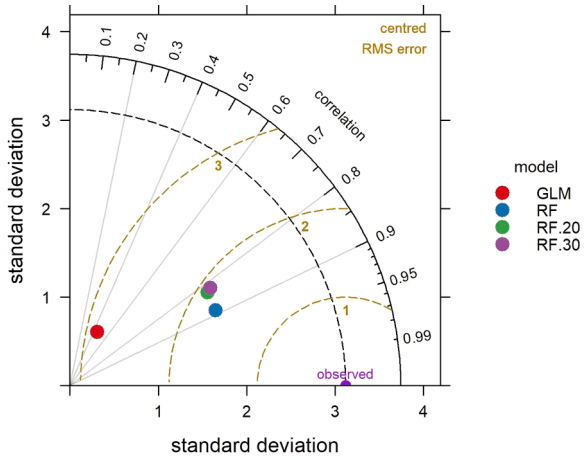

Fig. 8. Taylor diagram of soil water content (%) predicted by General Linear Model (GLM), Random Forest Regression (RF) with pixel-based sampling and with buffer-based means (RF.20 – 20 cm buffer, RF.30 – 30 m buffer) (surveys of 27.05.2019; 04.06.2019; 10.09.2020; 14.09.2020).

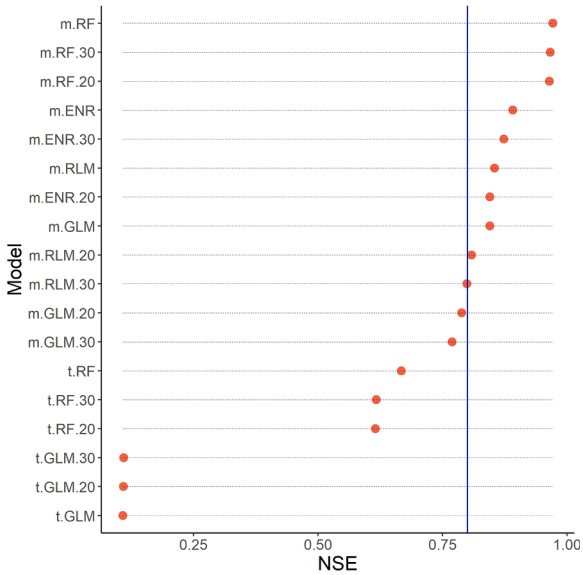

Fig. 9. Nash-Sutcliffe model efficiencies (NSE) of different predictions using General Linear Models (GLM), Robust Linear Models (RLM), Random Forest Regression (RF) and Elastic Net Regression (ENR) with multispectral (m.) and thermal (t.) data (models without numbers: pixel-based sampling, 0.20: mean values of 20 cm buffers around the sampling points, 0.30: mean values of 30 cm buffers around the sampling points).

also important. This result was similar to Hsu and Chang (2019), they found R^2s between 0.25 and 0.70, and the aerial images ensured an R^2 of 0.41., but their predictor variable was the temperature vegetation dryness index (TVDI), which is a relevant difference.

We found that the means of 20 or 30 cm radius buffers did not have relevant effect on accuracy. According to the RKCV measures, the buffered values had resulted in larger R^2s and RMSEs, but accuracy

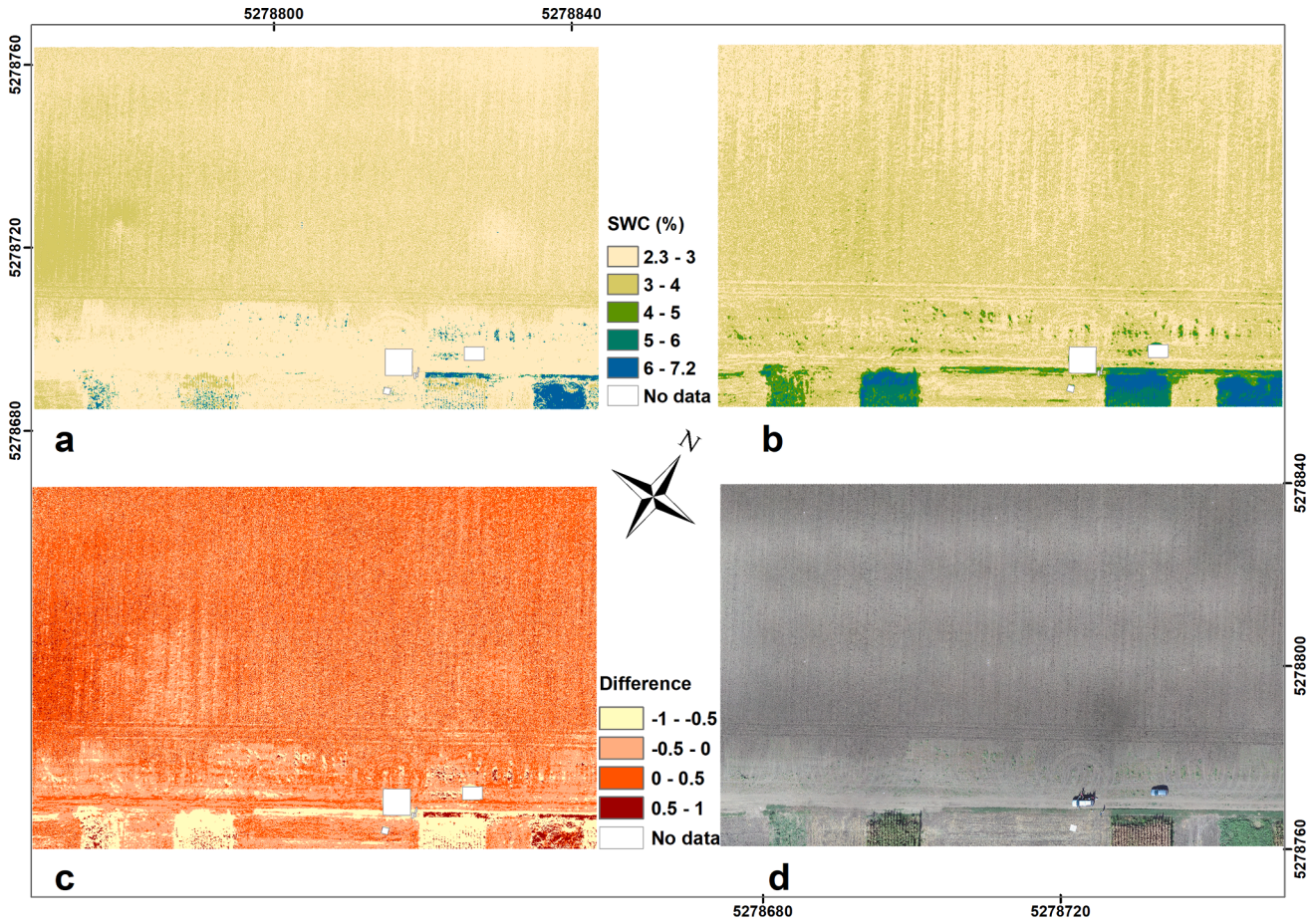

Fig. 10. Estimation of soil water content (SWC) with multispectral (a) and thermal (b) cameras with the difference of two estimations (c) and the UAV-based RGB orthomosaic of the plot (d). CRS: UTM34N.

testing with the testing dataset showed that extracting the single pixels are enough. Differences usually were within 1–2 %; thus, our hypothesis on the advantage of buffering was not true.

A precise timing of irrigation coupled with spatially partitioned dose of applied water are highly dependent on the spatial heterogeneity of SWC within the cultivated area in order to ensure the best water supply for the homogenous growth of all plants in the field (Abdelhaleem et al., 2021; Bortolini et al., 2018; Hao et al., 2022). Thus, irrigation have to be based on high spatial resolution and up-to-date data/map of the SWC. SWC data obtained from the gravimetric method is precise but even if spatially well-sampled, time consuming, expensive and slow (Little et al., 1998) and the outcome shows a state from the past and cannot support the planning of spatially partitioned water doses. Previous UAV studies revealed SWC can be mapped using UAV-based aerial surveys, but with the accuracies compared to the gravimetric method were varying (e.g., Wang et al., 2018; Hsu and Chang, 2019; Lu et al., 2020). Our approach indicated a good accuracy of RF regression algorithm and the detailed probability of the spatial heterogeneity map for SWC for multispectral cameras. Our maps provided appropriate SWC estimations according to the nRMSEs with high spatial resolution, which is an innovative step for precision agriculture not only for a more precise timing of irrigation, but it leads to more efficient water usage as a part of precision irrigation system. This can be reached with the help of the visualized spatial heterogeneities of SWC in large details which was provided by a machine learning approach of this study.

5. Conclusions

We aimed to reveal the efficiency of UAV-based thermal and multispectral cameras in SWC mapping using four machine learning algorithms and three types of pixel sampling. We found the following outcomes:

- Data of multispectral camera was efficient regarding both the medians (i.e., median of 30 models of the RKCV) of R^2 and nRMSE values (0.96 and ~ 10 %, respectively).
- Data of thermal camera ensured a median R^2 only of 0.71, and almost 25 % nRMSE.
- A single survey did not provide enough high variance neither for the predictors nor for target variable; accordingly, we advise to merge the data of different surveys of both the multispectral and thermal data collection campaigns.
- RF was the best regression algorithm, and in case of multispectral surveys, the ENR was also efficient (R^2s were 0.97 and 0.88, respectively).
- Single pixel-based sampling was an appropriate method to extract data from the images, means of 20 and 30 cm radius buffers did not help to gain better accuracy; RKCV (based on 30 models) and NSE (based on an independent testing dataset) showed different results.

Although UAV-based SWC mapping can have prediction errors, the spatial heterogeneity can be revealed in detail, which helps the farmers or agricultural managers to increase the efficacy of planning irrigation in precision agriculture.

Declaration of Competing Interest

The authors declare that they have no known competing financial

interests or personal relationships that could have appeared to influence the work reported in this paper.

Acknowledgments

This research was funded by the NKFIH TNN 123457 and NKFIH K 131478 project and the Thematic Excellence Programme (TKP2020-NKA-04) of the Ministry for Innovation and Technology in Hungary. This research was also influenced by the COST Action CA16219 "HARMONIOUS - Harmonization of UAS techniques for agricultural and natural ecosystems monitoring".

References

Abdelhaleem, F.S., Basiouny, M., Ashour, E., Mahmoud, A., 2021. Application of remote sensing and geographic information systems in irrigation water management under water scarcity conditions in Fayoum. Egypt. J. Environ. Manage. 299, 113683 https://doi.org/10.1016/j.jenvman.2021.113683.

Abu-Hamdeh, N.H., Reeder, R.C., 2000. Soil thermal conductivity effects of density, moisture, salt concentration, and organic matter. Soil Sci. Soc. Am. J. 64, 1285–1290. https://doi.org/10.2136/sssaj2000.6441285x.

Al-Naji, A., Fakhri, A.B., Gharghan, S.K., Chahl, J., 2021. Soil color analysis based on a RGB camera and an artificial neural network towards smart irrigation: A pilot study. Heliyon 7, e06078. https://doi.org/10.1016/j.heliyon.2021.e06078.

Aragon, B., Johansen, K., Parkes, S., Malbeteau, Y., Al-Mashharawi, S., Al-Amoudi, T., Andrade, C.F., Turner, D., Lucieer, A., McCabe, M.F., 2020. A calibration procedure for field and UAV-Based uncooled thermal infrared instruments. Sensors 20, 3316. https://doi.org/10.3390/s20113316.

Ayoubi, S., Jabbari, M., Khademi, H., 2018. Multiple linear modeling between soil properties, magnetic susceptibility and heavy metals in various land uses. Model. Earth Syst. Environ. 4, 579–589. https://doi.org/10.1007/s40808-018-0442-0.

Babaeian, E., Sadeghi, M., Franz, T.E., Jones, S., Tuller, M., 2018. Mapping soil moisture with the OPtical TRApezoid Model (OPTRAM) based on long-term MODIS observations. Remote Sens. Environ. 211, 425–440. https://doi.org/10.1016/j.rse.2018.04.029.

Bai, X., Chen, Y., Chen, J., Cui, W., Tai, X., Zhang, Z., Cui, J., Ning, J., 2021. Optimal window size selection for spectral information extraction of sampling points from UAV multispectral images for soil moisture content inversion. Comput. Electron. Agric. 190, 106456 https://doi.org/10.1016/j.compag.2021.106456.

Baldwin, D., Manfreda, S., Keller, K., Smithwick, E.A.H., 2017. Predicting root zone soil moisture with soil properties and satellite near-surface moisture data across the conterminous United States. J. Hydrol. 546, 393–404. https://doi.org/10.1016/j.jhydrol.2017.01.020.

Baldwin, D., Manfreda, S., Lin, H., Smithwick, E.A.H., 2019. Estimating root zone soil moisture across the Eastern United States with Passive Microwave Satellite Data and a Simple Hydrologic Model. Remote Sens. 11 (17), 2013. https://doi.org/10.3390/rs11172013.

Barry-Macaulay, D., Bouazza, A., Wang, B., Singh, R.M., 2015. Evaluation of soil thermal conductivity models. Can. Geotech. J. 52, 1892–1900. https://doi.org/10.1139/cgj-2014-0518.

Baumann, P., Lee, J., Behrens, T., Biswas, A., Six, J., McLachlan, G., Viscarra Rossel, R.A., 2022. Modelling soil water retention and water-holding capacity with visible–near-infrared spectra and machine learning. European J. Soil Science 73. https://doi.org/10.1111/ejss.13220.

Bortolini, L., Maucieri, C., Borin, M., 2018. A Tool for the evaluation of irrigation water quality in the arid and semi-arid regions. Agronomy 8, 23. https://doi.org/10.3390/agronomy8020023.

Brownlee, J., 2016. Machine Learning Mastery With R: Get Started. Build Accurate Models and Work Through Projects Step-by-Step, Machine Learning Mastery.

Carslaw, D.C., Ropkins, K., 2012. openair - An R package for air quality data analysis. Environ. Modell. Software 27–28, 52–61. https://doi.org/10.1016/j.envsoft.2011.09.008.

D'Odorico, P., Chiarelli, D.D., Rosa, L., Bini, A., Zilberman, D., Rulli, M.C., 2020. The global value of water in agriculture. Proc. Natl. Acad. Sci. U.S.A. 117, 21985–21993. https://doi.org/10.1073/pnas.2005835117.

Field, A.P., Miles, J., Field, Z., 2012. Discovering statistics using R. Thousand Oaks, Calif, Sage, London.

Fox, J., 1997. Applied regression analysis, linear models, and related methods. Sage Publications, Thousand Oaks, Calif.

Friedman, J., Hastie, T., Tibshirani, R., 2010. Regularization Paths for Generalized Linear Models via Coordinate Descent. J. Stat. Soft. 33. https://doi.org/10.18637/jss.v033.i01.

Ge, X., Ding, J., Jin, X., Wang, J., Chen, X., Li, X., Liu, J., Xie, B., 2021. Estimating agricultural soil moisture content through UAV-based hyperspectral images in the arid region. Remote Sens. 13, 1562. https://doi.org/10.3390/rs13081562.

Gu, H., Lin, Z., Guo, W., Deb, S., 2021. Retrieving surface soil water content using a soil texture adjusted vegetation index and unmanned aerial system images. Remote Sens. 13, 145. https://doi.org/10.3390/rs13010145.

Gupta, H.V., Kling, H., 2011. On typical range, sensitivity, and normalization of Mean Squared Error and Nash-Sutcliffe Efficiency type metrics: technical note. Water Resour. Res. 47, W10601. https://doi.org/10.1029/2011WR010962.

Hao, R., Huang, G., Liu, L., Li, Y., Li, J., Zhai, M., 2022. Sustainable conjunctive water management model for alleviating water shortage. J. Environ. Manage. 304, 114243 https://doi.org/10.1016/j.jenvman.2021.114243.

Hassanpour, R., Zarehaghi, D., Neyshabouri, M.R., Feizizadeh, B., Rahmati, M., 2020. Modification on optical trapezoid model for accurate estimation of soil moisture content in a maize growing field. J. Appl. Remote Sens. 14 https://doi.org/10.1117/1.JRS.14.034519.

Hsu, W.-L., Chang, K.-T., 2019. Cross-estimation of soil moisture using thermal infrared images with different resolutions. Sensors and Materials 31, 387. https://doi.org/10.18494/SAM.2019.2090.

Hu, W., Chau, H.W., Qiu, W., Si, B., 2017. Environmental controls on the spatial variability of soil water dynamics in a small watershed. J. Hydrol. 551, 47–55. https://doi.org/10.1016/j.jhydrol.2017.05.054.

Huuskonen, J., Oksanen, T., 2018. Soil sampling with drones and augmented reality in precision agriculture. Comput. Electron. Agric. 154, 25–35. https://doi.org/10.1016/j.compag.2018.08.039.

James, M.R., Chandler, J.H., Eltner, A., Fraser, C., Miller, P.E., Mills, J.P., Noble, T., Robson, S., Lane, S.N., 2019. Guidelines on the use of structure-from-motion photogrammetry in geomorphic research. Earth Surf. Process. Landforms 44, 2081–2084. https://doi.org/10.1002/esp.4637.

Kovács, A., Király, A., 2021. Assessment of climate change exposure of tourism in Hungary using observations and regional climate model data. HunGeoBull 70, 215–231. https://doi.org/10.15201/hungeobull.70.3.2.

Kuhn, M., Wing, J., Weston, S., Williams, A., Keefer, C., Engelhardt, A., Cooper, T., Mayer, Z., Kenkel, B., R Core Team, Benesty, M., Lescarbeau, R., Ziem, A., Scrucca, L., Tang, Y., Candan, C., Hunt, T. 2021. Package "caret": Classification and Regression Training. R package version 6.0-88. Available online: https://cran.r-project.org/web/packages/caret/caret.pdf (Accessed on: 01 November 2021.). URL (accessed 11.1.21).

Lei, F., Crow, W.T., Shen, H., Su, C.-H., Holmes, T.R.H., Parinussa, R.M., Wang, G., 2018. Assessment of the impact of spatial heterogeneity on microwave satellite soil moisture periodic error. Remote Sens. Environ. 205, 85–99. https://doi.org/10.1016/j.rse.2017.11.002.

Little, K.M., Metelerkamp, B., Smith, C.W., 1998. A comparison of three methods of soil water content determination. South African J. Plant Soil 15, 80–89. https://doi.org/10.1080/02571862.1998.10635121.

Lóki, J., 2020. Debrecen természetföldrajza. Debreceni Szemle 28 (2), 3–25.

Lu, F., Sun, Y., Hou, F., 2020. Using UAV visible images to estimate the soil moisture of steppe. Water 12, 2334. https://doi.org/10.3390/w12092334.

Maes, W., Huete, A., Steppe, K., 2017. Optimizing the processing of UAV-based thermal imagery. Remote Sens. 9, 476. https://doi.org/10.3390/rs9050476.

Maltese, A., Minacapilli, M., Cammalleri, C., Ciraolo, G., D'Asaro, F., 2010. A thermal inertia model for soil water content retrieval using thermal and multispectral images, in: Neale, C.M.U., Maltese, Antonino (Eds.), Presented at the Remote Sensing, Toulouse, France, p. 78241G. https://doi.org/10.1117/12.864672.

Manfreda, S., Brocca, L., Moramarco, T., Melone, F., Sheffield, J., 2014. A physically based approach for the estimation of root-zone soil moisture from surface measurements. Hydrol. Earth Syst. Sci. 18, 1199–1212. https://doi.org/10.5194/hess-18-1199-2014.

Manfreda, S., McCabe, M., Miller, P., Lucas, R., Pajuelo Madrigal, V., Mallinis, G., Ben Dor, E., Helman, D., Estes, L., Ciraolo, G., Müllerová, J., Tauro, F., de Lima, M., de Lima, J., Maltese, A., Frances, F., Caylor, K., Kohv, M., Perks, M., Ruiz-Pérez, G., Su, Z., Vico, G., Toth, B., 2018. On the use of unmanned aerial systems for environmental monitoring. Remote Sens. 10, 641. https://doi.org/10.3390/rs10040641.

Matese, A., Toscano, P., Di Gennaro, S.F., Genesio, L., Vaccari, F.P., Primicerio, J., Belli, C., Zaldei, A., Bianconi, R., Gioli, B., 2015. Intercomparison of UAV, Aircraft and Satellite Remote Sensing Platforms for Precision Viticulture. Remote Sens. 7, 2971–2990. https://doi.org/10.3390/rs70302971.

McCuen, R.H., Knight, Z., Cutter, A.G., 2006. Evaluation of the Nash-Sutcliffe Efficiency Index. J. Hydrol. Eng. 11, 597–602. https://doi.org/10.1061/(ASCE)1084-0699(2006)11:6(597).

Messina, G., Modica, G., 2020. Applications of UAV thermal imagery in precision agriculture: state of the art and future research outlook. Remote Sens. 12, 1491. https://doi.org/10.3390/rs12091491.

Minacapilli, M., Cammalleri, C., Ciraolo, G., D'Asaro, F., Iovino, M., Maltese, A., 2012. Thermal inertia modeling for soil surface water content estimation: A laboratory experiment. Soil Sci. Soc. Am. J. 76, 92–100. https://doi.org/10.2136/sssaj2011.0122.

Moriasi, D.N., Gitau, M.W., Pai, N., Daggupati, P., 2015. Hydrologic and water quality models: performance measures and evaluation criteria. Trans. ASABE 58, 1763–1785. https://doi.org/10.13031/trans.58.10715.

Mukherjee, A., Misra, S., Raghuwanshi, N.S., 2019. A survey of unmanned aerial sensing solutions in precision agriculture. J. Netw. Comput. Appl. 148, 102461 https://doi.org/10.1016/j.jnca.2019.102461.

Naimi, S., Ayoubi, S., Demattê, J.A.M., Zeraatpisheh, M., Amorim, M.T.A., de Mello, F.A., O.,, 2021. Spatial prediction of soil surface properties in an arid region using synthetic soil image and machine learning. Geocarto International 1–24. https://doi.org/10.1080/10106049.2021.1996639.

Négyesi, G., Szabó, S., Buró, B., Mohammed, S., Lóki, J., Rajkai, K., Holb, I.J., 2021. Influence of soil moisture and crust formation on soil evaporation rate: A wind tunnel experiment in Hungary. Agronomy 11, 935. https://doi.org/10.3390/agronomy11050935.

Nikoosokhan, S., Nowamooz, H., Chazallon, C., 2016. Effect of dry density, soil texture and time-spatial variable water content on the soil thermal conductivity. Geomech. Geoeng. 11, 149–158. https://doi.org/10.1080/17486025.2015.1048313.

Petropoulos, G., Carlson, T.N., Wooster, M.J., Islam, S., 2009. A review of Ts/VI remote sensing based methods for the retrieval of land surface energy fluxes and soil surface moisture. Progress Physical Geography: Earth Environ. 33, 224–250. https://doi.org/10.1177/0309133309338997.

Petropoulos, G.P., Ireland, G., Barrett, B., 2015. Surface soil moisture retrievals from remote sensing: Current status, products & future trends. Physics and Chemistry of the Earth, Parts A/B/C 83–84, 36–56. https://doi.org/10.1016/j.pce.2015.02.009.

Pye, K., Tsoar, H., 2009. In: Aeolian Sand and Sand Dunes. Springer Berlin Heidelberg, Berlin, Heidelberg, pp. 175–253.

Robust Regression | R Data Analysis Examples. UCLA: Statistical Consulting Group. https://stats.idre.ucla.edu/r/dae/robust-regression/ (Accessed on 5 November 2021.). URL (accessed 11.5.21).

Romano, N., 2014. Soil moisture at local scale: Measurements and simulations. J. Hydrol. 516, 6–20. https://doi.org/10.1016/j.jhydrol.2014.01.026.

Sabaghy, S., Walker, J.P., Renzullo, L.J., Jackson, T.J., 2018. Spatially enhanced passive microwave derived soil moisture: Capabilities and opportunities. Remote Sens. Environ. 209, 551–580. https://doi.org/10.1016/j.rse.2018.02.065.

Sadeghi, M., Babaeian, E., Tuller, M., Jones, S.B., 2017. The optical trapezoid model: A novel approach to remote sensing of soil moisture applied to Sentinel-2 and Landsat-8 observations. Remote Sens. Environ. 198, 52–68. https://doi.org/10.1016/j.rse.2017.05.041.

Seo, M.-G., Shin, H.-S., Tsourdos, A., 2020. Soil moisture retrieval from airborne multispectral and infrared images using Convolutional Neural Network. IFAC-PapersOnLine 53, 15852–15857. https://doi.org/10.1016/j.ifacol.2020.12.240.

Soil Survey Staf, 2014. Keys to soil taxonomy, 12th ed. USDA-Natural Resources Conservation Service, Washington, DC, p. 3.

Szabó, G., Bertalan, L., Barkóczi, N., Kovács, Z., Burai, P., Lénárt, C., 2018. Zooming on Aerial Survey. In: Casagrande, G., Sik, A., Szabó, G. (Eds.), Small Flying Drones. Springer International Publishing, Cham, pp. 91–126. https://doi.org/10.1007/978-3-319-66577-1_4.

Tajik, S., Ayoubi, S., Nourbakhsh, F., 2012. Prediction of soil enzymes activity by Digital Terrain Analysis: Comparing Artificial Neural Network and Multiple Linear Regression Models. Environ. Engineer. Sci. 29, 798–806. https://doi.org/10.1089/ees.2011.0313.

Tajik, S., Ayoubi, S., Shirani, H., Zeraatpisheh, M., 2019. Digital mapping of soil invertebrates using environmental attributes in a deciduous forest ecosystem. Geoderma 353, 252–263. https://doi.org/10.1016/j.geoderma.2019.07.005.

Taylor, K.E., 2001. Summarizing multiple aspects of model performance in a single diagram. J. Geophys. Res. 106, 7183–7192. https://doi.org/10.1029/2000JD900719.

RPubs by RStudio, 2021. erblast/ Björn Oettinghaus. https://rpubs.com/erblast/ (Accessed on 17 November 2021).

Therneau, T., Atkinson, B., Ripley, B. 2019. rpart: Recursive Partitioning and Regression Trees. R package version 4.1-15. Available online: https://cran.r-project.org/web/packages/rpart/rpart.pdf (Accessed on: 01 November 2021.).

Tmušić, G., Manfreda, S., Aasen, H., James, M.R., Gonçalves, G., Ben-Dor, E., Brook, A., Polinova, M., Arranz, J.J., Mészáros, J., Zhuang, R., Johansen, K., Malbeteau, Y., de Lima, I.P., Davids, C., Herban, S., McCabe, M.F., 2020. Current practices in UAS-based environmental monitoring. Remote Sens. 12, 1001. https://doi.org/10.3390/rs12061001.

Van De Griend, A.A., Camillo, P.J., Gurney, R.J., 1985. Discrimination of soil physical parameters, thermal inertia, and soil moisture from diurnal surface temperature fluctuations. Water Resour. Res. 21, 997–1009. https://doi.org/10.1029/WR021i007p00997.

Venables, W.N., Ripley, B.D., Venables, W.N., 2002. Modern applied statistics with S, 4th, ed. ed. Statistics and computing, Springer, New York.

Vereecken, H., Huisman, J.A., Pachepsky, Y., Montzka, C., van der Kruk, J., Bogena, H., Weihermüller, L., Herbst, M., Martinez, G., Vanderborght, J., 2014. On the spatio-temporal dynamics of soil moisture at the field scale. J. Hydrol. 516, 76–96. https://doi.org/10.1016/j.jhydrol.2013.11.061.

Virtue, J., Turner, D., Williams, G., Zeliadt, S., McCabe, M., Lucieer, A., 2021. Thermal sensor calibration for unmanned aerial systems using an external heated shutter. Drones 5, 119. https://doi.org/10.3390/drones5040119.

Wang, S., Garcia, M., Ibrom, A., Jakobsen, J., Josef Köppl, C., Mallick, K., Looms, M., Bauer-Gottwein, P., 2018. Mapping root-zone soil moisture using a temperature–vegetation triangle approach with an unmanned aerial system: incorporating surface roughness from structure from motion. Remote Sens. 10, 1978. https://doi.org/10.3390/rs10121978.

Wang, Y., Shao, M., Liu, Z., Warrington, D.N., 2012. Regional spatial pattern of deep soil water content and its influencing factors. Hydrol. Sci. J. 57, 265–281. https://doi.org/10.1080/02626667.2011.644243.

Wigmore, O., Mark, B., McKenzie, J., Baraer, M., Lautz, L., 2019. Sub-metre mapping of surface soil moisture in proglacial valleys of the tropical Andes using a multispectral unmanned aerial vehicle. Remote Sens. Environ. 222, 104–118. https://doi.org/10.1016/j.rse.2018.12.024.

Yadav, S.K., Singh, P., Jadaun, S.P.S., Kumar, N., Upadhyay, R.K., 2019. Soil moisture analysis of Lalitpur district Uttar Pradesh India using Landsat and Sentinel data. International Archives of Photogrammetry, Remote Sensing and Spatial. Inf. Sci. XLII-3/W6, 351–356. https://doi.org/10.5194/isprs-archives-XLII-3-W6-351-2019.

Zambrano-Bigiarini, M., 2020. Zenodo. hzambran/hydroGOF, v0.4-0. https://doi.org/10.5281/ZENODO.839854.

Zeraatpisheh, M., Ayoubi, S., Mirbagheri, Z., Mosaddeghi, M.R., Xu, M., 2021. Spatial prediction of soil aggregate stability and soil organic carbon in aggregate fractions using machine learning algorithms and environmental variables. Geoderma Regional 27, e00440.

Zeraatpisheh, M., Garosi, Y., Reza Owliaie, H., Ayoubi, S., Taghizadeh-Mehrjardi, R., Scholten, T., Xu, M., 2022. Improving the spatial prediction of soil organic carbon using environmental covariates selection: A comparison of a group of environmental covariates. Catena 208, 105723. https://doi.org/10.1016/j.catena.2021.105723.

Zhang, J., Qiu, X., Wu, Y., Zhu, Y., Cao, Q., Liu, X., Cao, W., 2021. Combining texture, color, and vegetation indices from fixed-wing UAS imagery to estimate wheat growth parameters using multivariate regression methods. Comput. Electron. Agric. 185, 106138 https://doi.org/10.1016/j.compag.2021.106138.

Zhuang, R., Zeng, Y., Manfreda, S., Su, Z., 2020. Quantifying long-term land surface and root zone soil moisture over Tibetan Plateau. Remote Sens. 12, 509. https://doi.org/10.3390/rs12030509.